Particle Production and Hydrodynamic Flow: Recent Results from E877 for Au+Au Collisions at AGS Energy

Johannes P. Wessels for the E877 Collaboration:

J. Barrette[a], R. Bellwied[b], S. Bennett[b], R. Bersch[c], P. Braun-Munzinger[d], W. C. Chang[c], W. E. Cleland[e], M. Clemen[e], J. Cole[f], T. M. Cormier[b], Y. Dai[a], G. David[g], J. Dee[c], O. Dietzsch[h], M. Drigert[f], S. Esumi[i], A. French[b], K. Filimonov[a], J. R. Hall[b], T. K. Hemmick[c], N. Herrmann[d], B. Hong[c], S. Johnson[c], Y. Kwon[c], R. Lacasse[a], Q. Li[b], T. W. Ludlam[g], S. K. Mark[a], R. Matheus[b], S. McCorkle[g], D. Miśkowiec[d], J. T. Murgatroyd[b], E. O'Brien[g], S. Panitkin[c], V. Pantuev[c], P. Paul[c], T. Piazza[c], M. Pollack[c], C. Pruneau[b], Y. Qi[a], E. Reber[f], M. Rosati[a], N. C. daSilva[h], S. Sedykh[c], J. Sheen[b], U. Sonnadara[e], J. Stachel[i], N. Starinsky[a], E. M. Takagui[h], M. Trzaska[c], S.A. Voloshin[i*], T. Vongpaseuth[c], G. Wang[a], J. P. Wessels[i], C. L. Woody[g], N. Xu[c], Y. Zhang[c], C. Zou[c]

[a] McGill University, Montreal, Canada
[b] Wayne State University, Detroit, USA
[c] State University of New York, Stony Brook, USA
[d] Gesellschaft für Schwerionenforschung, Darmstadt, Germany
[e] University of Pittsburgh, Pittsburgh, USA
[f] Idaho National Engineering Laboratory, Idaho Falls, USA
[g] Brookhaven National Laboratory, Upton, USA
[h] University of São Paulo, Brazil
[i] University of Heidelberg, Heidelberg, Germany

In this article recent results of the E877 collaboration are presented. They include double differential multiplicities and rapidity densities of hadrons produced in Au+Au collisions at 11 AGeV/c, two-particle correlations of like and unlike particles, as well as some recent results on particle flow.

1. INTRODUCTION

Until the conclusion of its experimental program, experiment E877 recorded $2 \cdot 10^6$, $1 \cdot 10^7$, and $2 \cdot 10^7$ central ($\sigma_{\rm top}/\sigma_{\rm geo} \approx 14\%$) Au+Au collisions at 11 AGeV/c in '93, '94, and '95, respectively. Here, we will present our latest results from the analysis of kaons, antiprotons, and the production of light nuclei. In conjunction with earlier results [1] and results presented by other collaborations at the AGS [2–5], there is now a rather complete systematics for hadron production available for Au+Au collisions at 11 AGeV/c. It was presented in P. Braun-Munzinger's experimental overview talk at this conference

*On leave from Moscow Engineering Physics Institute, Moscow, 115409, Russia

[6]. There it was concluded that, for central collisions, the rapidity distributions can be well reproduced with the assumption of longitudinal flow, and the transverse mass (m_t) spectra indicate the presence of strong transverse flow. After a brief description of the experimental setup we show some results on hadron spectra and yields. In the section on particle flow in non-central collisions, we will concentrate on the flow of identified particles with respect to the reaction plane. A summary of the ongoing investigations of correlations of like, as well as unlike particles will conclude this report.

2. EXPERIMENTAL SETUP

The setup of the experiment (Fig. 1) employs nearly 4π-calorimetry which can be used for event characterization and the reconstruction of the event plane (see e.g. [7,8]). The highly segmented target (TCAL) and participant calorimeters (PCAL) cover the pseudorapidity (η) ranges $-0.5 < \eta_{\mathrm{TCAL}} < 0.8$ and $0.8 < \eta_{\mathrm{PCAL}} < 4.2$ respectively. They record the transverse energy (E_t) produced in the collision by means of which the centrality is deduced, while the forward uranium calorimeter (UCAL) measures the remaining energy in a small cone around zero degrees.

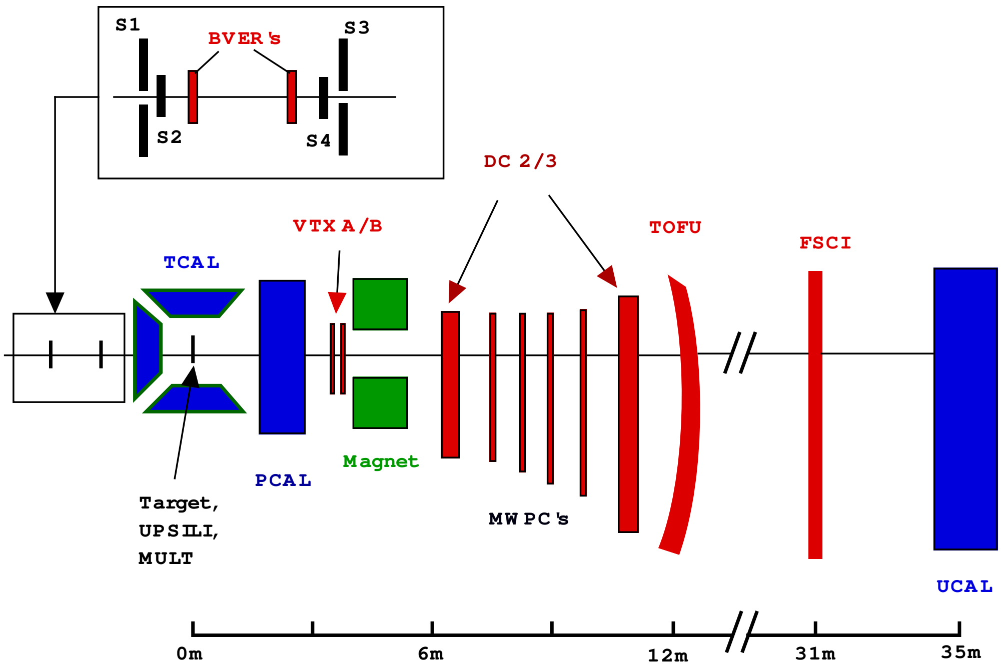

Fig. 1. Schematic drawing of the E877 Setup

The position of the beam on target and the time of impact are reconstructed using two Si-strip detectors (BVER) upstream of the target and a set of start and veto counters (S1-4). The positions of particles emerging from a collision that pass through a steel collimator inside the PCAL ($-134 < \theta_{\mathrm{horizontal}} < 16$ mrad, $-11 < \theta_{\mathrm{vertical}} < 11$ mrad) are recorded in two vertex chambers (VTXA,B) before the magnet and a set of drift chambers (DC2,3) and multi-wire proportional chambers (MWPCs) after the magnet. Their time of flight is recorded in two scintillator walls (TOFU,FSCI). The particles are identified in the spectrometer through a measurement of their momentum and velocity. The mass resolution is quantitatively understood in terms of the bending power, position resolution, multiple scattering and time of flight resolution ($\sigma_{\text{tof}} \approx 85$ ps). The momentum resolution is limited to $\Delta p/p \approx 3\%$ due to multiple scattering. The acceptance of the spectrometer for the various particle species is shown in Fig. 2.

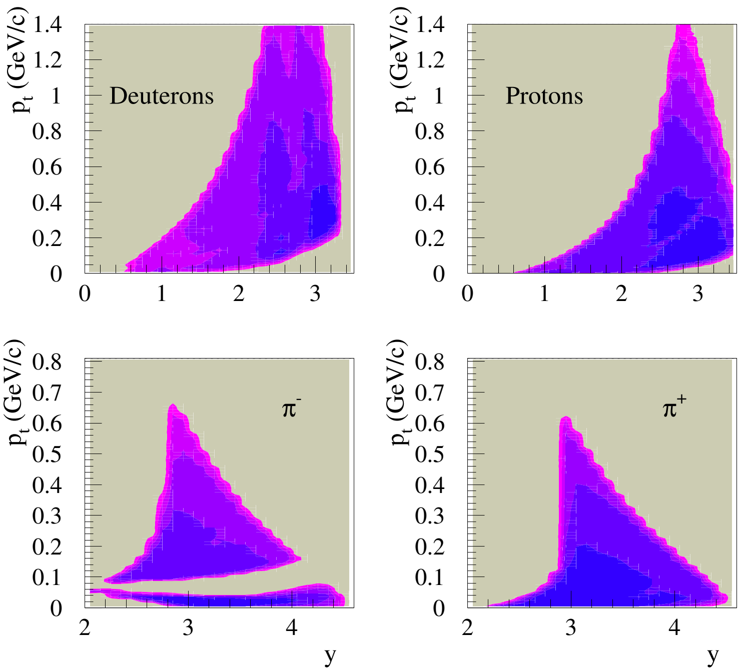

Fig. 2. Acceptance for deuterons, protons, negative, and positive pions (the magnetic field was optimized for the acceptance of positive particles).

3. HADRON SPECTRA AND YIELDS

The rapidity distributions and transverse mass spectra of pions and protons were presented in detail at the last Quark Matter conference [1]. In conjunction with the data of other experiments [3] it was possible to deduce the phase space integrated particle ratios. These were then compared [10] to a thermal model [11] calculation. Good agreement between data and calculation was found for source temperatures T=120-140 MeV and a baryon chemical potential of μ_{B}=540 MeV. Already for the lighter system (Si+(Al)Pb) it was noted that the measured slope parameters of transverse mass spectra at midrapidity were distinctly different from these temperatures and were scaling with the mass of the particle. This can be ascribed to the presence of transverse flow. Furthermore, the slopes of all particles increased in going to the heavier Au+Au system. This observation is consistent with a larger flow present in the heavier system.

Since the multiplicity of pions and protons is large, small contaminations of kaons in the respective spectra hardly alter their shape. The converse of this is not true. It is especially difficult to cleanly identify kaons with low transverse momenta. For the '94 run of the experiment additional tracking chambers (VTXA,B) upstream of the magnet were therefore installed. Furthermore, the tracking scheme was adapted to find for each each particle trajectory the correct vertex. As before, an upper momentum limit of 4 GeV/c was imposed. This led to a clean kaon sample at rapidities $2.3 \leq \text{y}_{\text{cm}} \leq 2.5$.

The resulting, fully corrected, transverse mass spectra are depicted in Fig. 3. Starting at the bin y=2.5 the spectra are scaled by successive factors of ten. They are evaluated for the 4% most central collisions. Although the range in m_t is rather limited, the extracted slopes are compatible within errors with those measured in [3]. For comparison, the K^- data are plotted together with results from [3] reflected about midrapidity ($y_{cm} = 1.6$). The data sets agree well in the region of overlap, both in slope and absolute yield. The positive kaons show a distinct dip at the lowest m_t. This can probably be ascribed to Coulomb repulsion between the kaons and the net positive charge of the fireball. This issue will be further discussed when we turn to the ratios of positive and negative pions.

Since the slopes and the rapidity distributions of positive and negative kaons are very similar, the ratio K^+/K^- can be deduced from our measurements. The experimentally observed value is $K^+/K^- = 3.8 \pm 0.95$. This is in agreement with the value calculated with the thermal model [11] of 4.6(4.3) for a temperature of 120(140) MeV and a chemical potential quoted above.

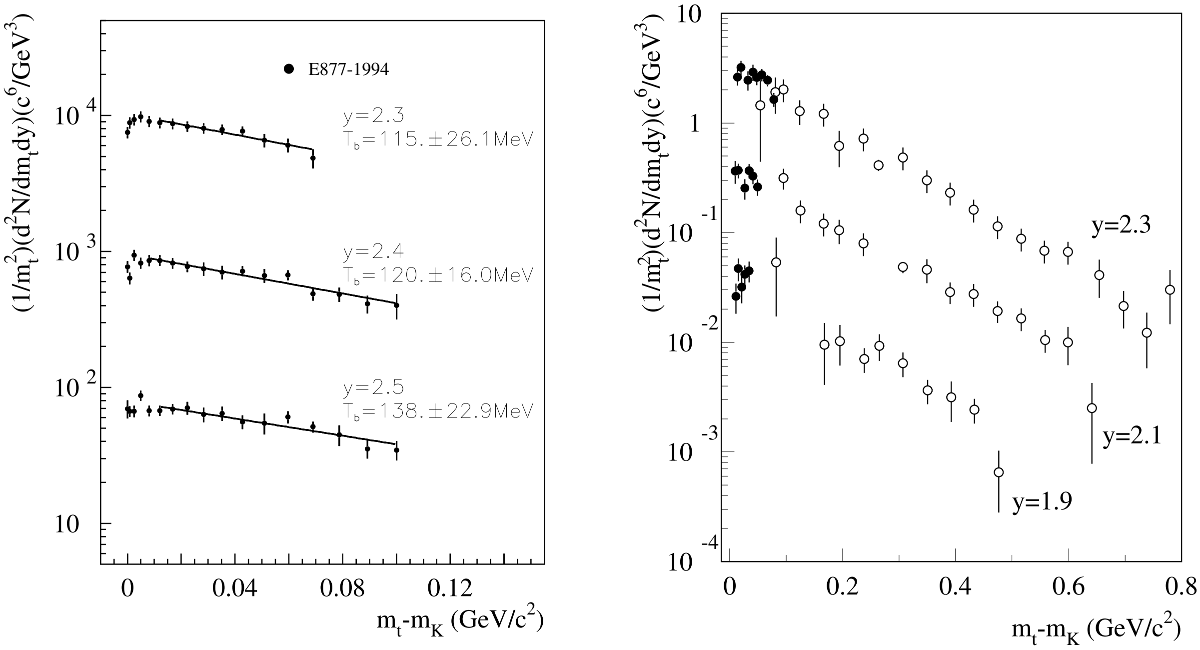

Fig. 3. Transverse mass spectra of positive (left) and negative (right) kaons. The open symbols are results of the E866 collaboration [9] which were reflected about midrapidity for comparison.

The above mentioned vertex chambers were also instrumental in cleanly identifying antiprotons. The measured invariant multiplicity is shown in Fig. 4 together with results of other experiments ([4] and refs. therein). The centrality selection for the analysis of antiprotons was the top 10% of the cross section. The final sample of 47 antiprotons was coming from interactions with an average centrality of 4%.

There is obviously some discrepancy between experiments on the yield of antiprotons at low p_t. The clue to this may lie in the fact that the various experiments have different acceptance for anti-protons from weak decays (e.g. $\bar{\Lambda}, \Sigma^-, \overline{\Xi}^o, \Xi^+$). This has been studied extensively [12] for the experimental setup of E877. Because of the large mass asymmetry in these decays, the $\bar{p}$ points back to the target. It is reconstructed for 70% of the $\bar{\Lambda}$

and for 100% of the Σ^- decaying such that the $\bar{\mathrm{p}}$ is emitted into the acceptance of the spectrometer. Our measured yield is in agreement with results by the E864 and E866 collaboration. The apparent discrepancy to the data of E878 may have to do with their lower detection probability for $\bar{\mathrm{p}}$ from decays. We measure a ratio of $\bar{\mathrm{p}}/\mathrm{p} = (4.4 \pm 0.8) \cdot 10^{-4}$, again in good agreement with thermal model predictions of $1.5 \cdot 10^{-4}(5.8 \cdot 10^{-4})$ for temperatures of 120(140) MeV including all $\bar{\mathrm{p}}$ from decays.

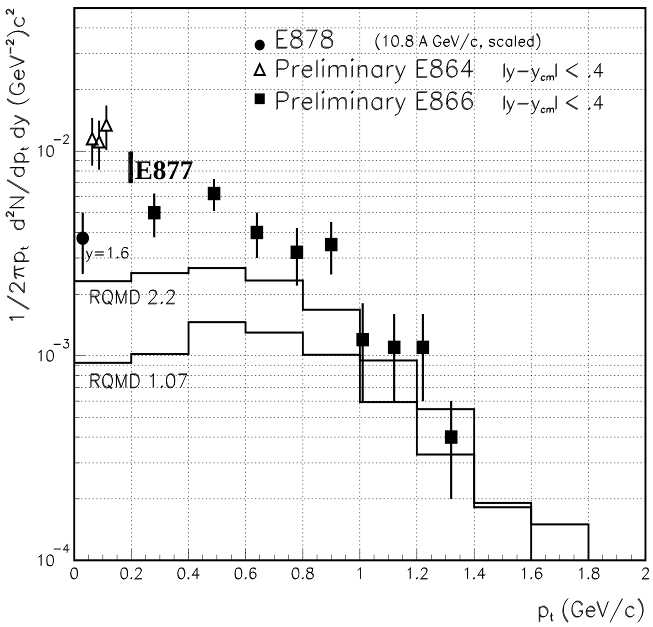

Fig. 4. Invariant multiplicity of anti-protons at midrapidity. The compilation of data and model calculations was done by J.G. Lajoie [4]. The E877 data point has been added as a band at $\mathrm{p_t} = 0.2$ GeV/c. The vertical band corresponds to $\pm 1\sigma_{\mathrm{stat.}}$.

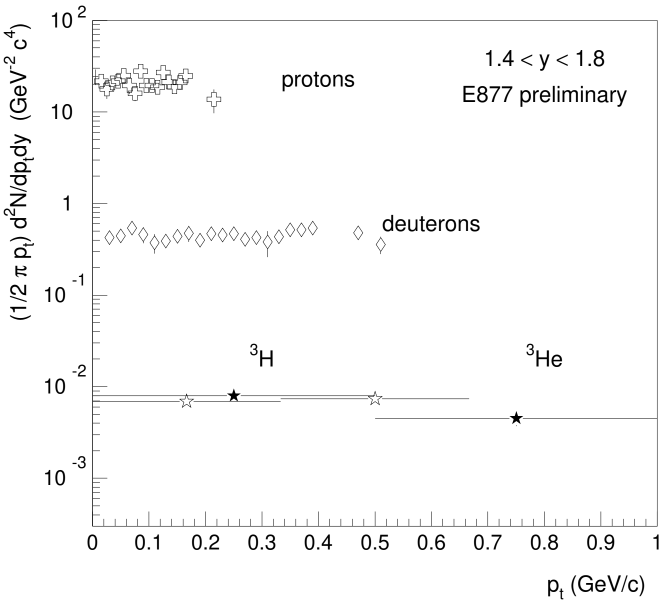

Fig. 5. Invariant multiplicity of protons(crosses), deuterons(diamonds), tritons(open stars), and ^{3}He(solid stars) at midrapidity for the 4% most central events.

First results on deuteron production have been presented previously [1]. The study of heavy particles has now been extended to include also tritons and Helium isotopes. Fig. 5 shows the invariant multiplicities of deuterons, tritons, and ^{3}He at midrapidity in comparison to proton data. The spectra are, again, evaluated for the 4% most central events. The cross sections for deuterons is reduced by a factor of 50 compared to that for protons. The cross sections for tritons and ^{3}He are comparable and again suppressed by a factor of 50 compared to that for deuterons. This is expected for a system with very high entropy and leads to a natural explanation of their production in terms of coalescence or thermal models [13]. In [14] the measured proton spectra were reproduced by varying the temperature (T) and radius parameter (R) of a flowing thermal source [15]. A coalescence formalism [16] was then used to construct the deuteron spectra.

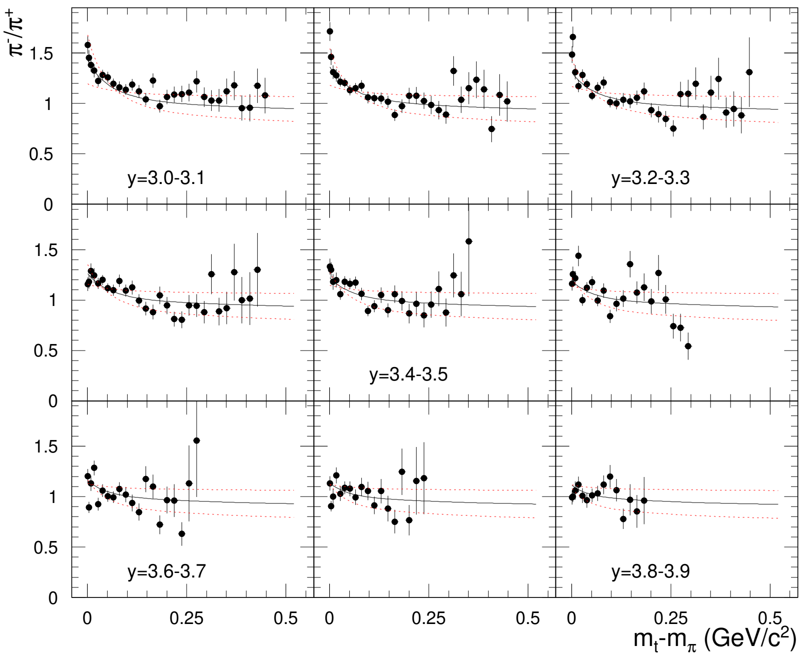

Fig. 6. Ratios of transverse mass spectra of negative over positive pions from the 4% most central events for different rapidity intervals. (The dotted lines indicate the errors on the fitted solid line. See text for details.)

By exploring the parameter space (T,R) to best match the observed deuteron spectra the size of the emitting source could be characterized. The resulting temperature and radius parameter ($\mathrm{R} = \sigma_{\mathrm{x}} = \sigma_{\mathrm{y}} = \sigma_{\mathrm{z}}$, i.e. variance of a 3d-Gaussian in each dimension) were found to be $\mathrm{T} = 137^{+38}_{-12}$ MeV and $\mathrm{R} = 6.5^{+1.7}_{-.4}$ fm.

That Coulomb effects may play a role in the description of the measured $\mathrm{m_t}$-spectra was already mentioned in the discussion of the kaon spectra. Also, it was shown that the π^-/π^+-ratio at a given momentum is sensitive to the presence of a charged central source [17]:

$$\frac{\pi^-}{\pi^+}(\mathrm{p}) = \mathrm{F} \cdot \frac{\sqrt{\mathrm{p}^2 + 2\mathrm{E}(\mathrm{p})\mathrm{V_C} + \mathrm{V_C}^2}}{\sqrt{\mathrm{p}^2 - 2\mathrm{E}(\mathrm{p})\mathrm{V_C} + \mathrm{V_C}^2}} \cdot \frac{\mathrm{E}(\mathrm{p}) + \mathrm{V_C}}{\mathrm{E}(\mathrm{p}) - \mathrm{V_C}} \cdot \frac{\mathrm{n}(\mathrm{p_i^-})}{\mathrm{n}(\mathrm{p_i^+})} \tag{1}$$

where $n(p_i^-), n(p_i^+)$ are the multiplicities of π^-, π^+ with initial momenta p_i, F is an overall normalization factor and V_c is the Coulomb potential of the central source. The ratios of transverse mass spectra of π^- over π^+ are shown in Fig. 6. A clear rise of the data at low m_t can be seen. The influence of weak decays of Λs (e.g. $\Lambda \rightarrow p\pi^-$) on these ratios was studied with RQMD [18] events and found to be small. The π^-/π^+-ratios in Fig. 6 were fitted according to the above equation with $V_c = 31 \pm 22$ MeV and $F = 0.92 \pm 0.14$.

4. FLOW OF IDENTIFIED PARTICLES

The observed change in the slope parameter of transverse mass spectra of different mass particles for the most central collisions is indicative of the presence of strong transverse flow [11,19]. After having established the anisotropic sideward flow [20] E877 has focused on studying this phenomenon, which was well known from lower energies, as a function of the centrality of the collision and the transverse momentum for different species of emitted particles. The latest results on this analysis were presented by S. Voloshin in a separate contribution to this conference [21]. A method based on the Fourier expansion of azimuthal distributions was devised [8,7,22] in order to reconstruct the reaction plane and to measure the anisotropy of particle emission with respect to it. The amplitudes of the harmonics of this expansion v_n correspond to the strength of the anisotropic flow. The first harmonic v_1 corresponds to the *sideward* flow, v_2 is now called *elliptic* flow.

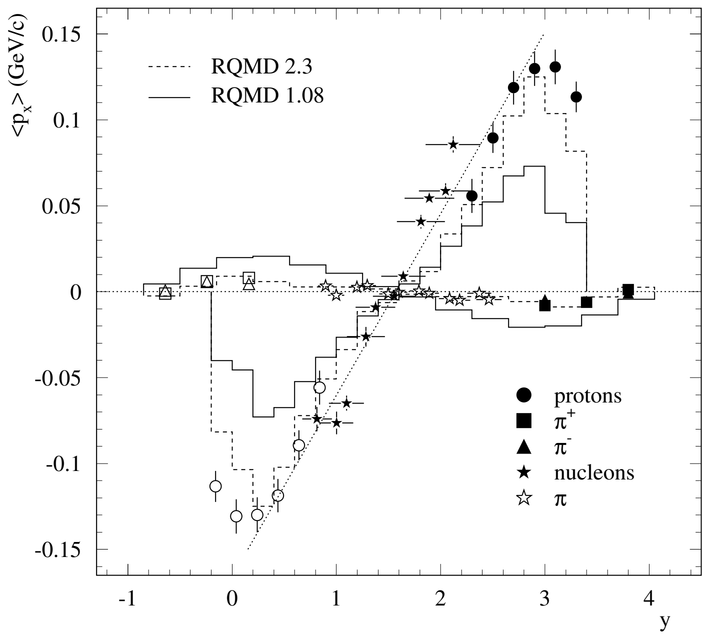

Fig. 7. Projection of the average transverse momentum of protons and pions onto the reaction plane as a function of rapidity for the centrality where the sideward flow is largest($\sigma_{top}/\sigma_{geo} = 13-9\%$). Protons (circles) and charged pions (squares, triangles) are identified in the spectrometer (open symbols are reflected about midrapidity), stars depict results from a measurement of transverse energy and charged multiplicity (for details see [7,8]).

Integrating and weighting with p_t the measured distributions of $v_n(p_t)$ for different particles yields their average momentum $\langle p_x \rangle$ in the reaction plane. The results of this integration are shown in Fig. 7 for protons and charged pions. The measurement in the spectrometer is complemented by the values for nucleon and pion flow, determined through disentangling their respective contributions to the observed azimuthal anisotropy of transverse energy and charged particle multiplicity. The dotted line through midrapidity is drawn to help judging the degree of antisymmetry of the values $\langle p_x \rangle$ for nucleons. Protons exhibit the largest value of $\langle p_x \rangle$ of about 130 MeV/c at beam rapidity. For charged pions $\langle p_x \rangle$ is smaller by a factor of 20 and of opposite sign. This is dominantly governed by low p_t pions. As can be seen in Fig. 8, v_1 of e.g. positive pions turns positive for higher transverse momenta, i.e. they flow in the same direction as the protons. This fact is hidden by the integral measurement of the average momentum $\langle p_x \rangle$ in the reaction plane as shown in Fig. 7. The rather complicated shape of the $v_1(p_t)$ distribution may be explained by a superposition of effects: Coulomb interaction with a central source (as discussed above), absorption, and an overall transverse movement of the emitting source [23].

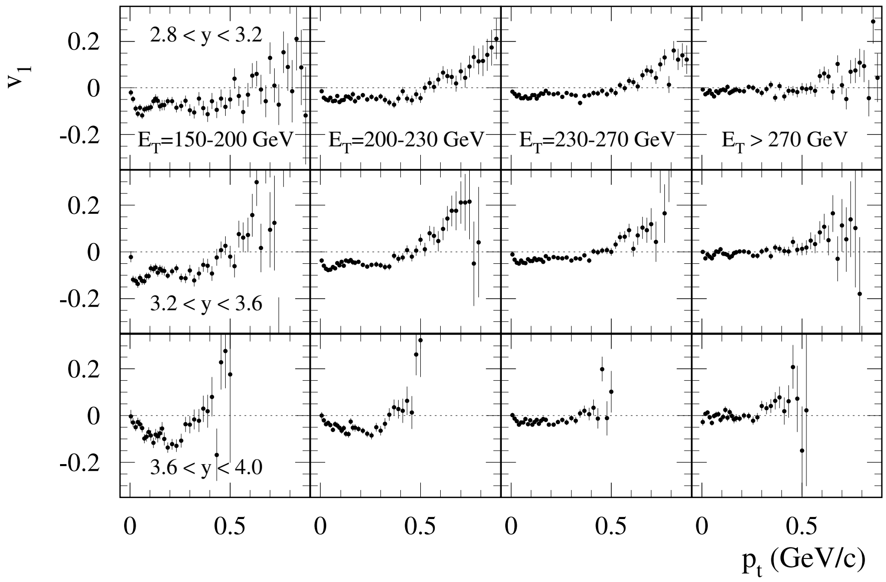

Fig. 8. Transverse momentum dependence for the first moment v_1 of the π^+ azimuthal distribution for different rapidities and centralities of the collision as defined in table 1 of [21]. (From [8].)

In Fig. 7 our measurements of $\langle p_x \rangle$ are compared to results of two RQMD calculations (versions 1.08 [18] and 2.3 [24]). Version 1.08 has been run in cascade mode (solid line). Generally, the magnitude of $\langle p_x \rangle$ for protons is underpredicted by almost a factor of two at beam rapidity, while the magnitude of $\langle p_x \rangle$ of pions is overpredicted by a factor of 2-3. Meanwhile mean-field type potentials have been included in version 2.3 and good agreement with this integrated measurement is found.

In Fig. 9, looking still more differentially, the results of the same calculations are compared to the measured values of v_1 for protons as a function of p_t for different rapidity intervals and the same centrality used in Fig. 7. There it becomes evident that, while the $\langle p_x \rangle$ is well reproduced by RQMD 2.3, the p_t dependence of v_1 is not properly described. It has been noted in [8] that the observed shape of this distribution is the one expected for a transversely moving thermal source.

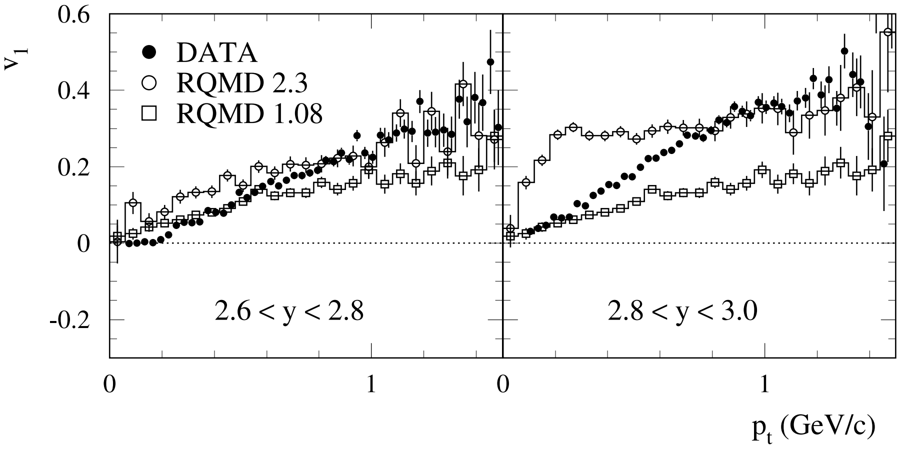

Fig. 9. Comparison of the transverse momentum dependence of v_1 for protons for different rapidities with those predicted by two versions of RQMD (at the same centrality as in Fig. 7) (From [8]).

5. TWO-PARTICLE CORRELATIONS

Two-particle correlations were used to determine the phase space distribution of pions at freeze-out. For this purpose, three-dimensional correlation functions of identical pions were analyzed in the standard (‘*out-side-long*’) coordinates [25]. It was concluded, that the system had undergone significant expansion before freeze-out, well in line with the flow results presented above. Furthermore, the extracted source parameters were used to calculate the average phase space density of pions at freeze-out. The obtained densities (0.1-0.25 π/phase space cell at the measured rapidities) were found to be consistent with the assumption of the pions being emitted from a source in local thermal equilibrium.

The procedure of extracting source parameters was crucially depending on a careful correction of the measured correlation function for Coulomb final state interaction, momentum resolution, and two-track acceptance in the spectrometer. Recently, we developed a new analysis approach in which we compare the ‘*raw*’ correlation functions C_2 (i.e. uncorrected for Coulomb final state interaction) with the results of Monte-Carlo simulations (Fig. 10). In the calculations, pairs of particles were generated, each particle characterized by four space-time and three momentum coordinates. The space-time coordinates were sampled according to source functions for pions (S_π) and protons (S_p):

$$S_\pi \sim f \cdot \exp\left(-\frac{x^2+y^2}{2R_T^2} - \frac{z^2}{2R_z^2} - \frac{t^2}{2\tau^2}\right) + (1-f)\cdot \exp\left(-\frac{r^2}{2R_{halo}^2} - \frac{t^2}{2\tau_{halo}^2}\right) \qquad (2)$$

$$S_p \sim \exp\left(-\frac{r^2}{2R^2}\right) \qquad (3)$$

The correlation functions of identical particles (left panel of Fig. 10) could be reproduced using $f = 0.65$ as probability for direct emission of pions, transverse radius $R_T = 4$ fm, longitudinal radius $R_z = 5$ fm, lifetime $\tau = 2$ fm/c, radius of the halo for decay from long lived resonances $R_{halo} = 18$ fm, with a lifetime $\tau_{halo} = 18$ fm/c. The radius of the proton source was $R = 4$ fm. The values for all radii correspond to variances of

Gaussian in one dimension. The momenta were generated according to the experimentally observed distributions. For each pair a weighting factor was calculated based on the code by Lednicky [26] accounting for Bose-Einstein (or Fermi) correlations, mutual Coulomb interaction, and strong interaction. Subsequently, they were propagated through the spectrometer, also taking into account finite detector resolution, multiple scattering, and a track separation dependent detection efficiency.

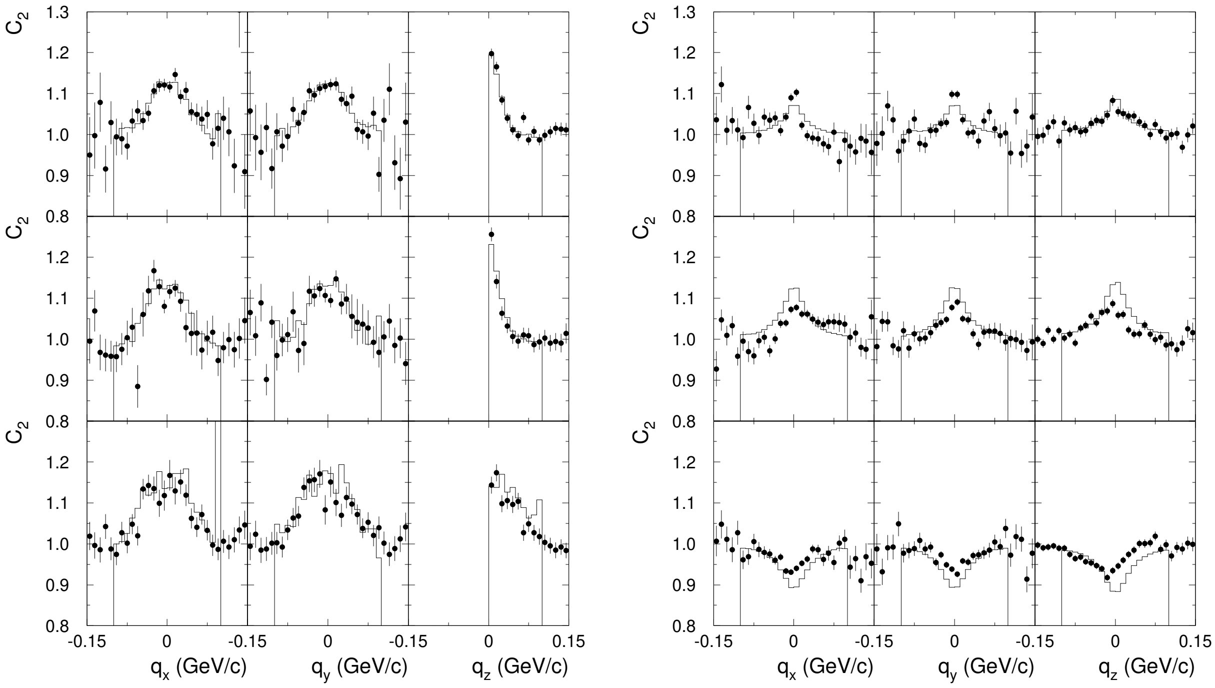

Fig. 10. Projections of measured uncorrected three-dimensional correlation functions (data points) compared to generated '*raw*' correlation functions for pairs with $\langle y \rangle = 0.5$ and transverse rapidity $y_t < 0.5$ ($y_t = 0.5 \log((m_t + p_t)/(m_t - p_t))$): left) top - $\pi^+\pi^+$; middle - $\pi^-\pi^-$; bottom - pp, right) top - $\pi^+\pi^-$; middle - π^-p; bottom: π^+p. (q_x is in the reaction plane, $q_z = q_{long}$, and q_y is perpendicular to both.)

The correlation functions of non-identical particles, generated with the same source parameters (Fig. 10 right panel), fail to reproduce the asymmetric shape of the experimentally observed pion-proton correlation function in the direction of q_z. Such an asymmetry in the non-identical particle correlation function indicates a finite separation between the sources of the two particles [26,27]. We found that, by advancing the proton source by 10 fm from the pion source in beam direction, a reasonable description of the unlike pair correlation functions can be achieved. This is illustrated in Fig. 11. The identical pair correlation functions are, of course, not affected by this displacement.

Two-dimensional correlation functions were studied as a function of the average transverse mass of the pair (m_T). The results from $\pi^+\pi^+$- and K^+K^+-correlations are shown in Fig. 12. The transverse radii (R_T) are found to systematically decrease with increasing transverse mass of the pair and increasing rapidity of the pair. This behavior is consistent with the assumption of a collectively expanding system. The result from the K^+K^+-correlation function follow the trend although it is taken at slightly different rapidity.

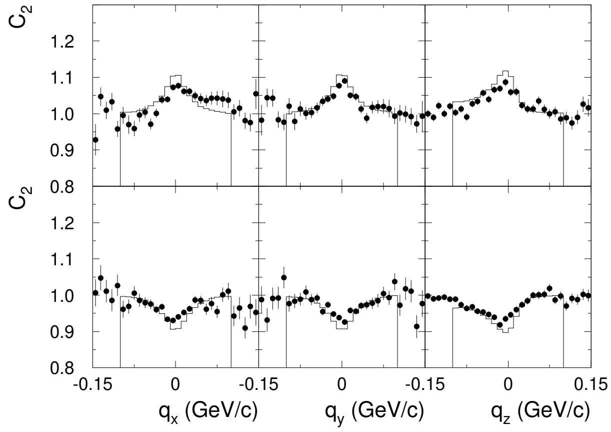

Fig. 11. Projections of measured uncorrected 3-dimensional correlation functions (data points) compared to generated 'raw' correlations for π^-p-pairs(top) and π^+p-pairs(bottom) assuming a shift of 10 fm along the beam direction of the proton relative to the pion source.

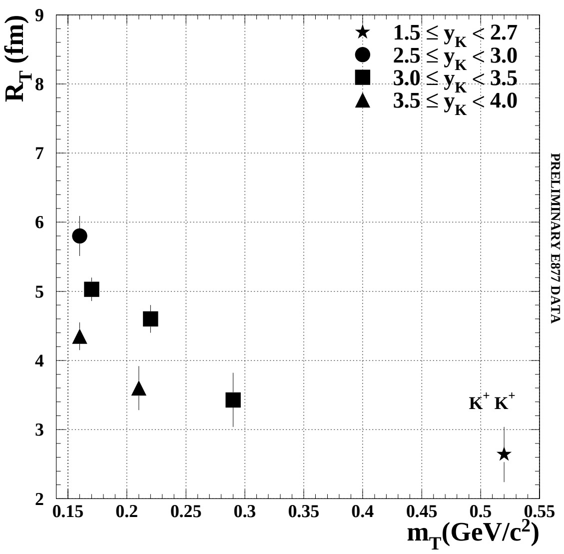

Fig. 12. Transverse radius (R_T) from 2-dimensional $\pi^+\pi^+$-correlations as a function of the transverse mass of the pair (m_T) for different pair rapidities. Also shown is the data point from K^+K^+-correlations (star).

6. SUMMARY AND OUTLOOK

We have presented our results on invariant multiplicities of kaons, antiprotons, deuterons, tritons, and ^{3}He. The ratios of K^+/K^- and $\bar{p}/p$ were found to be compatible with thermal model calculations implying equilibrium at chemical freeze-out. The yield of deuterons was shown to be sensitive to the temperature and radius of the emitting system at freeze-out. Ratios of π^-/π^+ at low m_t are sensitive to the Coulomb potential of the central source. Final results on the sideward flow of protons and pions were shown, and it was pointed out how, through differential comparisons of the data to models, one can learn about the dynamics of the emission. An analysis of 3-dimensional correlation functions of like and unlike particles was presented. Using source functions to reproduce the data, it was shown how the correlations of π^-p and π^+p can be described when their sources are displaced along the beam axis. The scaling of the transverse radius of emitted

$\pi^+\pi^+$ pairs with the transverse mass of the pair and its average rapidity is consistent with the scenario of a collectively expanding system.

In the future, with the much higher statistics available from the '95 run, we hope to be able to extend the correlation measurements to include the centrality and rapidity dependence as well as the correlation with the reaction plane. With the new vertex chambers a direct measurement of Λs and possibly $\bar{\Lambda}$s will be possible and the results will be included in our systematic study of particle flow at the AGS.

REFERENCES

1. R. Lacasse (E877 Collaboration), Nucl. Phys. **A610** (1996) 153c.
2. C. Ogilvie (E802, E859, E866, E917 Collaboration), Quark Matter '97, these proceedings.
3. Y. Akiba (E802, E866 Collaboration), Nucl. Phys. **A610** (1996) 139c.
4. J.G. Lajoie (E864 Collaboration), Proc. HIPAGS (1996) 59; C.A. Pruneau (E864 Collaboration), Quark Matter '97, these proceedings.
5. M.J. Bennett et al. (E878 Collaboration), Phys. Rev. **C56** (1997) 1521.
6. P. Braun-Munzinger, Quark Matter '97, these proceedings.
7. J. Barrette et al. (E877 Collaboration), Phys. Rev. **C55** (1997) 1420, **C56** (1997) 2336.
8. J. Barrette et al. (E877 Collaboration), Phys. Rev. **C56** (1997) 3254.
9. F. Wang (E864 Collaboration), Proc. HIPAGS (1996) 44.
10. J. Stachel, Nucl. Phys. **A610** (1996) 509c.
11. P. Braun-Munzinger, J. Stachel, J.P. Wessels, N. Xu, Phys. Lett. **B344** (1995) 43.
12. Y. Kwon, PhD Thesis, SUNY at Stony Brook, (1997).
13. P. Braun-Munzinger, J. Stachel, J. Phys. **G21** (1995) L17.
14. S.C. Johnson, PhD Thesis, SUNY at Stony Brook, (1997).
15. S. Chapman, J.R. Nix, U. Heinz, Phys. Rev. **C52** (1995) 2694.
16. R. Mattiello, H. Sorge, H. Stöcker, W. Greiner, Phys. Rev. **C53** (1996) 1443.
17. G. Baym, P. Braun-Munzinger, Nucl. Phys. **A610** (1996) 286c.
18. H. Sorge, A.v. Keitz, R. Mattiello, H. Stöcker, W. Greiner, Phys. Lett. **B243** (1990) 7.
19. N. Xu (NA44 Collaboration), Nucl. Phys. **A610** (1996) 175c.
20. J. Barrette et al. (E877 Collaboration), Phys. Rev. Lett. **73** (1994) 2532.
21. S.A. Voloshin, Quark Matter '97, these proceedings.
22. S.A. Voloshin, Y. Zhang, Z. Phys. **C70** (1996) 665.
23. S.A. Voloshin, Phys. Rev. **C55** (1997) R1630.
24. H. Sorge, Phys. Lett. **B402** (1997) 251.
25. D. Miśkowiec (E877 collaboration) Nucl. Phys. **A610** (1996) 227c; J. Barrette et al. (E877 Collaboration), Phys. Rev. Lett. **78** (1997) 2916.
26. R. Lednicky, V.L. Lyuboshitz, Sov. J. Nucl. Phys. **35** (1982) 770; R. Lednicky, V.L. Lyuboshitz, B. Erazmus, D. Nouais, preprint, SUBATECH-94-22, Nantes
27. S. Voloshin, R. Lednicky, S. Panitkin, N. Xu, Phys. Rev. Lett. **79** (1997) 4766.